Appl. Phys. B 71, 725–731 (2000) / Digital Object Identifier (DOI) 10.1007/s003400000436

Applied Physics B
Lasers
and Optics

Investigations in the TECFLAM swirling diffusion flame: Laser Raman measurements and CFD calculations

W. Meier*, O. Keck, B. Noll, O. Kunz, W. Stricker

DLR-Institut für Verbrennungstechnik, Pfaffenwaldring 38, 70569 Stuttgart, Germany
(Fax: +49-711/6862-578, E-mail: wolfgang.meier@dlr.de, berthold.noll@dlr.de, winfried.stricker@dlr.de)

Received: 19 April 2000/Revised version: 15 June 2000/Published online: 5 October 2000 –

Abstract. A standard burner for confined swirling natural gas flames is presented which was developed within the German TECFLAM cooperation. The aims of the TECFLAM research program are the establishment of an extensive experimental database from selective flames and the validation and improvement of mathematical combustion models. In this paper, results from joint PDF measurements of temperature, mixture fraction, and major species concentrations in a turbulent diffusion flame with 150 kW thermal load, equivalence ratio 0.833, and swirl number 0.9 are presented. Major aspects of the investigation are the general quantitative characterization of the flame and the study of the thermochemical state, e.g. effects of turbulence–chemistry interactions. Scatterplots of temperature, CH_4, and CO mole fractions as well as mean mixture fraction and temperature fields are presented and discussed. Furthermore, CFD calculations have been performed using the code Fluent 5 as an example of a commercially available code that is frequently used for technical applications. The comparison between the calculated and measured results reveals some significant deviations which are discussed with respect to the applicability of this code to swirling turbulent flames.

PACS: 33.20; 78.30; 82.40; 89.30

Swirling flows are widely applied in technical combustion systems in order to achieve a fast mixing of fuel and air and to stabilize the flame by recirculation of hot combustion products. The correct mathematical simulation of these flames is, however, difficult and belongs to the important and challenging tasks in modern computational fluid dynamics. In order to improve the experimental and theoretical knowledge of turbulent swirling diffusion flames the TECFLAM cooperation between several German universities and the DLR developed a burner for natural gas/air flames with a thermal power of typically 150 kW. The flames are confined by a water-cooled combustion chamber with good optical access for various measuring techniques. A number of well-defined "standard flames" have been investigated in identical copies of the burner at five different institutes with the goal to get an extensive and reliable quantitative characterization of the flames [1–5]. Great care was taken to ensure identical operating conditions of the flames and each research group contributed its specialized knowledge to achieve a high level of accuracy and confidence in the measurements. The results, comprising velocity, temperature, mixture fraction, species concentrations, and radiation, provide a detailed insight into the complex physical and chemical processes occurring in the combustion chamber and form a comprehensive basis for the validation of CFD codes.

At the German Aerospace Center (DLR) single-pulse spontaneous Raman scattering was applied to determine the joint probability density functions (PDFs) of the temperature, mixture fraction, and major species concentrations. The mean values and fluctuations derived from the PDFs yield a general characterization of the temperature and concentration fields, and the correlations between various quantities give an insight into the turbulence–chemistry interactions. Effects of finite-rate chemistry, flame stretch, mixing, and heat loss were studied in experiments performed in a flame with a Reynolds number of 42 900 and a swirl number of 0.9.

The comparison of the experimental data with numerical calculations reveals some significant disagreements which are mainly due to an incorrect simulation of the flow field. It was not the aim of this investigation to develop a new CFD code, but to test and assess the commonly available and frequently used Fluent 5 code with respect to its applicability to confined swirling diffusion flames.

1 Experiment

A schematic drawing of the burner and combustion chamber is shown in Fig. 1. Natural gas and air are supplied to the flame through annular nozzles with inside diam-

*Corresponding author.

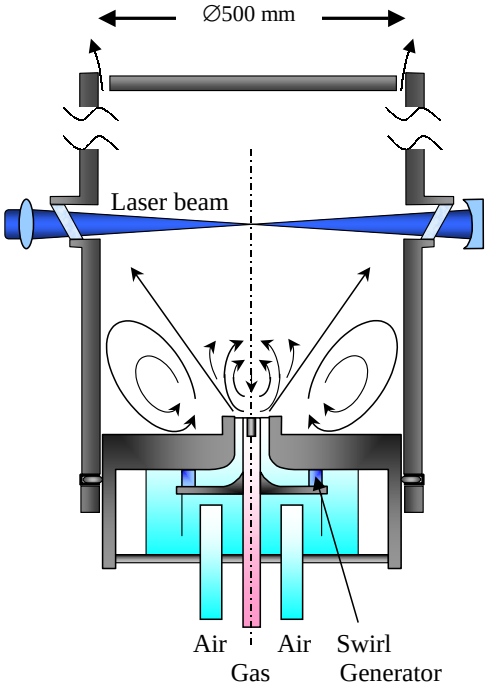

Fig. 1. Schematic drawing of the TECFLAM swirl burner

eter (i.d.) 20 mm, outside diameter (o.d.) 26 mm, and i.d. 30 mm, o.d. 60 mm, respectively. The natural gas contained 96.4%–98.2% CH_4 by volume and minor admixtures of N_2, CO_2, and higher hydrocarbons (changing from day to day). The air had a water vapor content of typically 0.8%. The swirl number of the air stream can be varied by a moveable block swirl generator inside the burner [6]. The flame investigated had a thermal power of 150 kW, an air/fuel ratio of $\lambda = 1.2$ (equivalence ratio 0.833), and a swirl number of $S = 0.9$. The corresponding Reynolds numbers were 42 900 at the air flow inlet and 7900 at the (non-swirled) fuel flow inlet. The water-cooled combustion chamber ($T_{\text{water,in}} \approx 65\,^{\circ}\text{C}$, $T_{\text{water,out}} \approx 75\,^{\circ}\text{C}$) has an i.d. of 500 mm, four windows for optical access, and an annular slit for the exhaust gas at the top. The burner can be moved vertically within the chamber like a piston by 500 mm in order to change the relative measuring height. The axial symmetry of the flame was experimentally checked and confirmed. Figure 1 also indicates the characteristics of the overall flow field which can be divided into three regimes: (i) the mixing zone between the fuel and air streams where combustion takes place predominantly, (ii) the inner recirculation zone around the flame axis, and (iii) the outer recirculation zone. More details about the burner and flame can be found on the Internet [1].

The Raman system, described in detail in previous publications [7, 8], is based on a flashlamp-pumped dye laser ($\lambda = 489$ nm, 2 µs pulse duration, 3 J pulse energy) whose beam is focused into the combustion chamber by a lens and retroreflected on the other side by a spherical mirror. The scattered light from the focal region is collected at 90° by an achromatic lens ($\varnothing = 100$ mm, $f = 300$ mm) and relayed to the entrance slit of a spectrograph. After spectral separation, the Raman signals from the major species CH_4, H_2, O_2, N_2, H_2O, CO_2, and CO are detected simultaneously by photomultiplier tubes, transferred to gated integrators, and finally stored and processed in a PC. The spatial resolution of the measurement is determined by the focal diameter of the laser beam and the slit width of the spectrograph and was 0.6 mm in each dimension.

In order to determine the number density of each species, the Raman signals were calibrated in cold and heated flows and in the exhaust gas of premixed laminar flames [8, 9]. The temperature was determined from the total number density via the ideal gas law, and the mixture fraction f was calculated using Bilger's definition [10, 11], which is based on the measured atomic mass fractions of O, H, and C. The data evaluation included corrections for cross talk between different Raman channels and background from laser-induced fluorescence from water and polycyclic hydrocarbons (PAHs). The background from laser-excited PAH emissions was corrected for by using the signals from additional photomultiplier tubes installed in Raman-free regions of the spectrum [8]. In the flame investigated the PAH concentrations were significantly smaller than in fuel-rich regions of jet diffusion flames [8], probably due to fast and efficient mixing of fuel and air by the swirling flow field which diminishes the formation of (large) PAHs. The accuracy achieved for the mean values is typically 2%–3% for the temperature, 2% for N_2, 4% for CO_2 and decreases for smaller mole fractions. The accuracy of a single-pulse measurement is reduced due to photon statistics and is on the order of 5% for the temperature, 5%–7% for H_2O (with a mole fraction of 0.2 at 2000 K), 12%–15% for O_2 (mole fraction 0.03, $T \approx 2000$ K), and 2% for CH_4 (mole fraction 1, $T \approx 1000$ K). The accuracy of the CO detection is lower than for the other species because of corrections for cross talk and interferences stemming from PAHs. For a CO mole fraction of 0.06 the accuracy of our measurements is 20%, for a mole fraction of 0.02 it is 50%. The investigation of the swirling flame was performed by recording series of 300 single-pulse measurements at eight different heights above the nozzle ($h = 10$ to 300 mm) and at radial locations ranging from −10 to 150 mm.

2 Numerical method

It should be emphasized that the primary intention of this work was not to elaborate or develop new combustion or turbulence models but to test the ability of current state-of-the-art codes to predict the behavior of swirling flames with a satisfactory accuracy. For this purpose the commercially available Fluent 5 code was used. Fluent 5 operates on the basis of finite-volume discretization and is able to work on structured as well as on unstructured computational grids. In the present study a two-dimensional grid for axis-symmetric flows was employed which consisted of roughly 180 grid points in axial and 80 grid points in radial direction. Thus, the whole chamber was discretized by about 14 000 computation cells. The results presented in this paper were gained on this grid and were found to be grid-independent by comparisons with much finer grids and with locally adapted grids. The discretization scheme employed was a second-order upwind scheme.

Fluent 5 offers a variety of different models for turbulence and combustion. Most of them were tested in the present work, however, in the case considered here, the results did not differ significantly. The presented results were obtained using

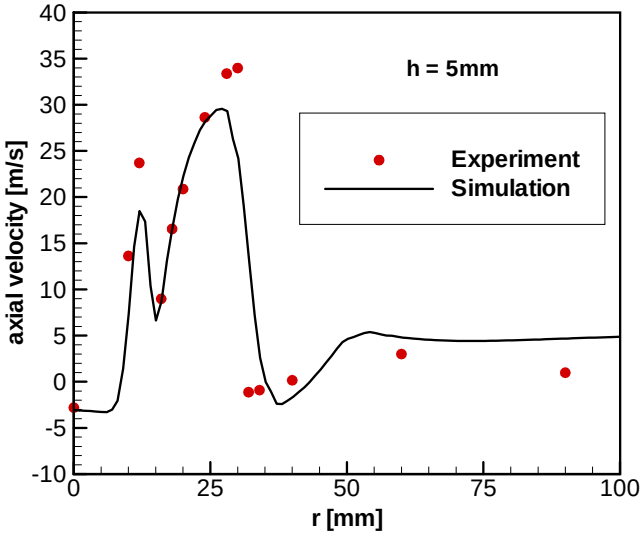

Fig. 2. Comparison between measured and simulated mean axial velocities at $h = 5$ mm

a Reynolds-stress turbulence model [12, 13] and a presumed β-pdf combustion model [14, 15]. Here, chemical equilibrium was assumed, which might not be adequate for all regions of the flame. However, further calculations on the base of a finite-rate chemistry model brought only small changes in the computed temperature fields. Due to relatively low wall temperatures, heat transfer by thermal radiation plays a significant role in the heat balance of the combustion chamber; therefore thermal radiation was included in the numerical simulations by a discrete-transfer radiation model [16]. The calculations revealed that the total heat loss due to radiation is about one third (≈ 50 kW) of the thermal power of the flame. This result was also confirmed by measurements [17]. However, it was found that radiation has no significant effect on the flow in the combustion region.

The inlet boundary was located at the burner mouth where fuel and air are injected separately thus giving well-defined boundary conditions for the flows. However, since the first plane of the velocity measurements was at a height of $h = 5$ mm above the burner mouth [5, 18] it was necessary to assume an inlet velocity distribution. In the present calculations the inlet velocity conditions were approximated by the measured velocities at $h = 5$ mm. The numerical calculations revealed that the velocity profiles at $h = 5$ mm do not differ significantly from those at the burner mouth. As an example, Fig. 2 shows a comparison of the radial profiles of the measured and calculated mean axial velocity at $h = 5$ mm.

3 Results and discussion

3.1 Thermochemical state of the flame

The most interesting and, as far as the simulation is concerned, difficult part of the flame is the flame root, where the highest flow velocities and smallest turbulent structures are present and where the flame is ignited and stabilized. The scatterplots in Fig. 3 show the measured correlations between temperature, CH_4, CO, and mixture fraction in this region at a height of 10 mm above the nozzle. Each symbol represents

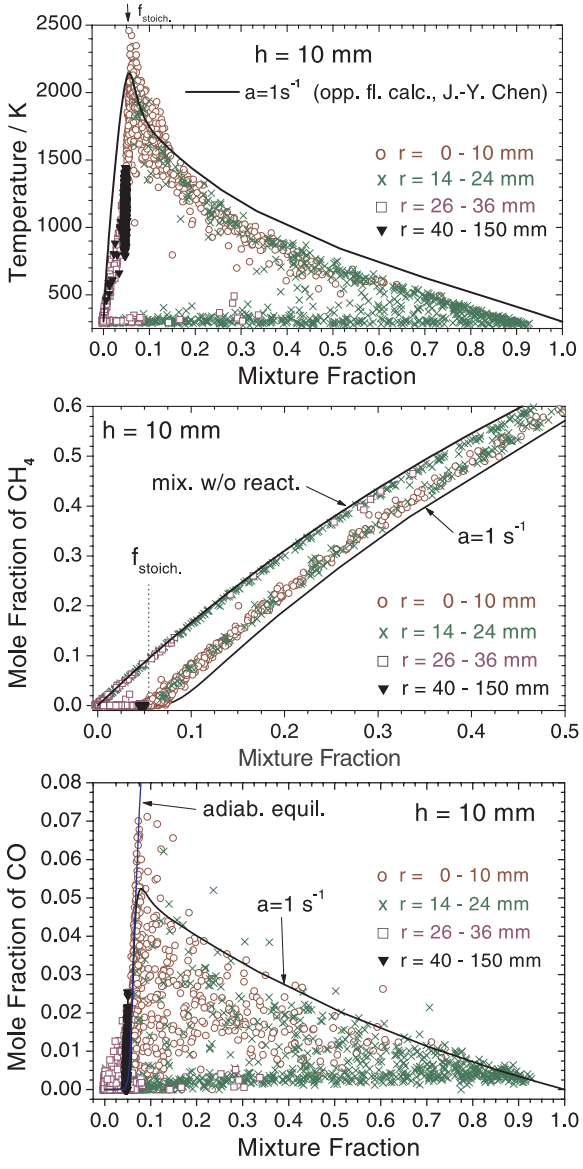

Fig. 3. Scatterplots of temperature, CH_4, and CO at $h = 10$ mm above the burner mouth. The different symbols represent different radial regions. Note that the mixture fraction axis is stretched in the middle frame in order to recognize details

the result of a single-pulse measurement, recorded at various radial locations. As an aid for the interpretation of the experimental data, the lines represent the result of a strained laminar opposed flame calculation with strain rate $a = 1\,\mathrm{s}^{-1}$ [19, 20], of adiabatic equilibrium (for CO), and of mixing without reaction (for CH_4). The calculations were performed for pure CH_4 and dry air and do, thus, not exactly match the natural gas/air composition used in the measurements.

At $r = 0$–10 mm (symbol ∘), stoichiometric and slightly rich mixtures ($f_{\mathrm{stoich.}} = 0.055$) with high temperatures prevail. Most of the temperature data points are scattered around the calculated laminar flame curve with $a = 1\,\mathrm{s}^{-1}$ indicating that the gas has completely reacted and that no significant temperature loss occurred. This region lies within the inner recirculation zone, where hot combustion products are transported from flame regions further downstream back to the burner mouth (see also right side of Fig. 7). The axial vel-

ocity changes direction at $r \approx 10$ mm [5, 18], but due to turbulent fluctuations there is, of course, no distinct separation between the inner recirculation zone and the adjacent inlet flow of natural gas. The corresponding CH_4 mole fractions (middle frame of Fig. 3, stretched f-axis) are roughly zero near $f_{\text{stoich.}}$ and increase stronger than the calculated values ($a = 1\,\text{s}^{-1}$) for fuel-rich mixtures. With respect to the classification of the data points into different flow regimes, the samples with $f > 0.075$ mark the transition to the group with $r = 14$–24 mm and are discussed later. With respect to CO (lower frame of Fig. 3), the highest mole fractions are found in the inner recirculation zone ($r = 0$–10 mm) where most of the samples are close to the calculated laminar opposed flame curve with $a = 1\,\text{s}^{-1}$. Calculations with high strain rates do not match the measured distribution for $f \leq f_{\text{stoich.}}$. A few samples exhibit mole fractions exceeding the values for $a = 1\,\text{s}^{-1}$ and tend to follow the adiabatic equilibrium curve. It should be mentioned that adiabatic equilibrium is usually not reached in fuel-rich regions of turbulent flames because the thermal decomposition of CH_4 takes a longer time than is typically available in turbulent flows. However, the residence time within the inner recirculation zone can be a few milliseconds, and at $T \approx 1900$–2000 K the approach of adiabatic equilibrium seems plausible.

Further outside ($r = 14$–24 mm, symbol x), samples with a wide spread in mixture fraction can be seen ranging almost from pure air ($f = 0$) to pure fuel ($f = 1$). This region lies above the fuel and air nozzles and the results reflect the different states of mixing (see Fig. 4). The temperatures are roughly divided into two branches: one at room temperature, i.e. unreacted mixtures, and the other close to the calculated temperature ($a = 1\,\text{s}^{-1}$). At first sight it seems surprising that even stoichiometric mixtures of fuel and air (around $r \approx 20$ mm) have not reacted. The chemical reaction is prevented by the high flow velocities and a too small heat and mass transfer from the inner recirculation zone. Also, the visible flame emission does not reach the burner but starts typically at $h \approx 20$–25 mm indicating that no combustion takes place below this height. This behavior is, however, plausible because the hot gases from the inner recirculation zone which initiate the flame reactions are shielded from potentially reactive CH_4/air mixtures by the inlet-flow of cold natural gas (see Fig. 4 for a schematic drawing of the situation).

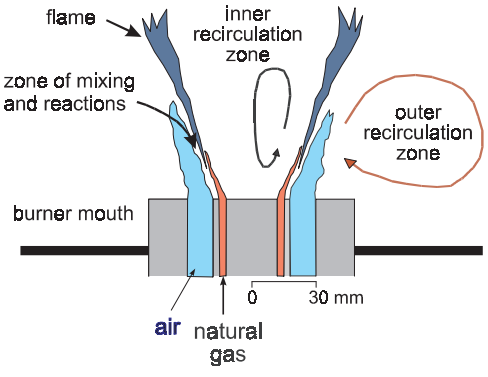

Fig. 4. Schematic drawing of the burner mouth and flow fields in the start region of the flame

The hot fuel-rich samples in this region ($r = 14$–24 mm) are mixtures of burnt gas from the inner recirculation zone with cold fuel and, in some samples, admixtures of air. The thermochemical state is mainly determined by mixing and to some degree by pyrolysis but scarcely by combustion reactions. The burnt gas contains no, or only little, O_2 (O_2 mole fraction < 0.02) so that combustion of CH_4 can not (or only partly) occur in this environment. Instead, the thermochemical state of the samples with high temperatures (> 1700–1800 K) is influenced by the thermal decomposition of CH_4 (pyrolysis) generating CO and H_2 and consuming CO_2. A calculation with CHEMKIN II for a perfectly stirred mixture of 5% CH_4 and 95% exhaust gas with $f = f_{\text{stoich.}}$ revealed that after 1 ms the CH_4 concentration dropped to 4.65% at 1700 K and to 2.53% at 1900 K [21]. The flow velocities near the burner mouth are typically 10–20 m/s (e.g. the axial velocity component was measured to be 14.5 m/s at $h = 10$ mm, $r = 12$ mm [5, 18]) corresponding to a distance of 10–20 mm traversed in 1 ms. Hence, the time scale of the natural gas flow at $h = 10$ mm and for mixing of fuel and burnt gas are on the same order of magnitude as the time scale of the thermal decomposition of CH_4 at $T > 1700$–1800 K. At lower temperatures pyrolysis should be of minor importance in this flame. The chemical state of the burnt gas/fuel mixtures is therefore expected to exhibit deviations from the calculation ($a = 1\,\text{s}^{-1}$) for $T \geq 1800$ K, $f \approx 0.055 - 0.09$ (the typical time scale for the strained flame with $a = 1\,\text{s}^{-1}$ is 0.1 s). The experimental results are in accordance with this picture: The measured CH_4 mole fractions are slightly larger than for $a = 1\,\text{s}^{-1}$ and the CO mole fractions (and also the H_2 mole fractions, not displayed) are lower than for $a = 1\,\text{s}^{-1}$. The scatter in the distributions reflects the competition between the varying time scales of residence time and CH_4 decomposition but are also, in the case of CO, influenced by the measurement uncertainty. The conditions favoring pyrolysis are given in the shear layer between natural gas and the inner recirculation zone when a small percent of CH_4 mixes with burnt gas. Further outside, the CH_4 mole fraction increases and the temperature decreases. For $f > 0.1$ ($T < 1700$ K) the measured temperatures are typically 100–200 K below the strained flame temperatures and the CH_4 mole fractions are about 0.03 above the calculated values. Most of these samples contain some O_2 (mole fraction < 0.04) originating from the air nozzle. The coexistence of fuel and oxidizer shows that these mixtures have not completely reacted and explains the temperature drop. However, it cannot be excluded that spatial averaging effects in the probe volume are also involved to a small degree (see discussion below). In addition, an analysis of the CH_4 and CO_2 measurements indicated a small shift of the mixture fraction axis by roughly 2%: the natural gas composition which enters the calculation of f was taken from the supplier's analysis and stated a CO_2 mole fraction of 0.002. The Raman measurements, on the other hand, resulted in a mole fraction of $0.008 - 0.01$. With this CO_2 concentration, the data points of the scatterplots would move by about 2% to higher f values, shifting the measured results closer to the calculated ones. The effect is, however, small and does not change the interpretation of the results.

One should bear in mind that due to the fast mixing the probed gas samples can have very different histories and a large variety of compositions of (partially) burnt gas, fuel,

and air. The interpretations given above are thus only a qualitative explanation of the thermochemical state.

In the region $r = 26$–36 mm (symbol □) the gas samples are fuel-lean and stem predominantly from mixtures of cold air with burnt gas from the outer recirculation zone. For larger radial positions ($r \geq 40$ mm, symbol ▼) this branch merges into a state of burnt gas with $f = 0.047$ which corresponds to the overall equivalence ratio of 0.833. The measuring location of these probes lies in the outer recirculation zone, and on the way there the molecules have lost heat to the chamber walls by radiation or convection so that the measured temperature is several hundred degrees below the adiabatic flame temperature.

Further downstream, at $h \approx 20$ mm, the natural gas flow becomes sufficiently diluted by turbulent mixing, so that the ignition and stabilization of the flame can take place. In comparison to $h = 10$ mm, the scatterplots at $h = 20$ and 40 mm (Fig. 5) have become narrower in mixture fraction space reflecting the rapid mixing in the flow. The different flame regimes mentioned above can still be distinguished and the thermochemical state of the probes from the inner (symbol ○, partly covered by x) and the outer (symbol ▼) recirculation zone has hardly changed in comparison to $h = 10$ mm. However, in the mixing region of the fuel and air streams the temperatures now cover the whole range from 300 K to 2300 K. The samples with intermediate temperatures can have two different histories: (1) They stem from local flame extinction leaving the gas in a partially reacted state. Local flame extinction certainly occurs in this flame and has been observed by visual inspection. (2) They are compositions of hot burnt gas and cold air/fuel mixtures which have not (yet) completely reacted. The experiments show a coexistence of oxygen and hydrocarbons for these samples but from the Raman measurements alone it cannot unambiguously be decided which of the two interpretations is correct.

The question arises whether the results could be influenced by spatial averaging effects, e.g. that fuel and air are present in different parts of the measuring volume ($\approx 0.6^3$ mm^3) but not mixed on the molecular level. The occurrence of inhomogeneous compositions within the probe volume, i.e. gradients of the mixture fraction or temperature, cannot be excluded. The pointwise Raman measurements and laser light sheet measurements of the fuel distribution with a spatial resolution of 0.15 mm revealed that the turbulent mixing of fuel and air is very rapid, so that at $h = 10$ mm pure fuel ($f = 1$) is no longer present. The light sheet experiments were performed using laser-induced fluorescence of NO which was seeded into the fuel as a tracer. From these measurements, the gradients of the fuel mole fraction were estimated to be smaller than 0.1 mm^{-1} for $h \geq 10$ mm. Thus, spatial averaging effects are small as far as mixing is concerned. On the other hand, laser light sheet measurements of OH radical distributions indicated that the regions with large gradients of OH concentrations (reflecting the reaction zones or at least the edge of it) are often smaller than 0.6 mm so that the temperature gradients within the measuring volume can be large. The probability that the reaction zone lies within the probe volume is, however, small: At $h = 40$ mm the reaction zone moves statistically from roughly $r = 20$ mm to $r = 40$ mm, as deduced from single-pulse planar OH images. Assuming a width of ≈ 0.3 mm for the regions with large OH gradients, the probability that this gradient lies within the probe volume is approx. $(0.6 + 0.3)/20 = 0.045$. In summary, spatial averaging can occur near $f_{\text{stoich.}}$ due to large gradients in the reaction zones but only a few samples are concerned which do not seem to alter the PDFs significantly.

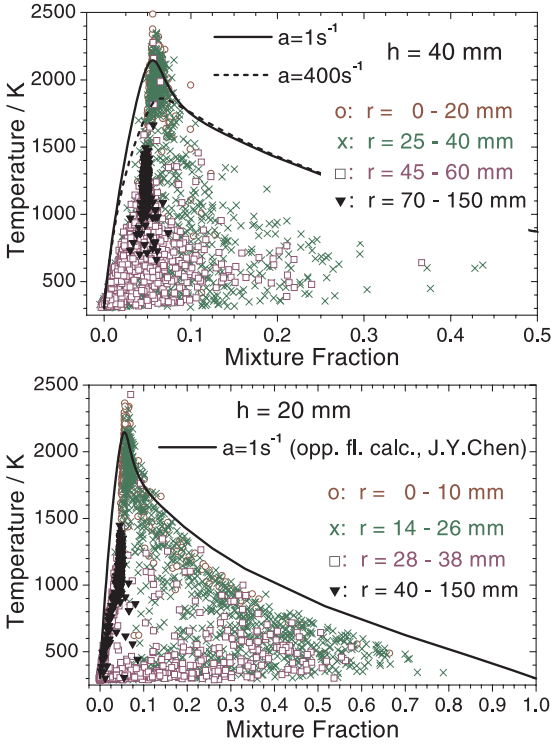

Fig. 5. Scatterplots of temperature at $h = 20$ and 40 mm

3.2 Mean values and comparison with numerical calculations

In order to illustrate the mixture fraction and temperature field, the mean values from measurements at 130 points were interpolated to generate two-dimensional distributions. The measured mixture fraction field is shown on the right-hand

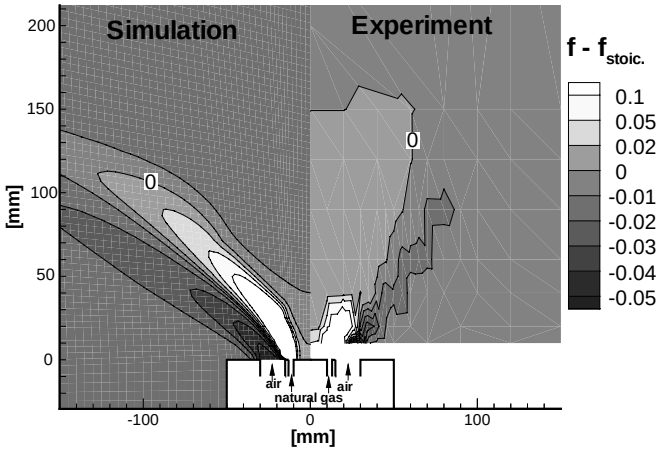

Fig. 6. Two-dimensional distribution of Favre-averaged mean mixture fractions. *Right side*: experiment, *left side*: simulation. Only the central part around the burner mouth is displayed (the diameter of the combustion chamber is 500 mm)

side of Fig. 6. The highest and lowest f values are observed above the fuel and air nozzle, respectively, and the shape of the regions with clearly fuel-rich or fuel-lean mixtures reflects the main direction of the flow field in this vertical plane. The contour lines also indicate the different regimes of the flame: The mixing region with the steepest gradients of the mixture fraction, the outer recirculation zone where the (final) mixture fraction of $f = 0.047$ ($\Phi = 0.833$) was measured (this region extends beyond the measured radial positions), and the inner recirculation zone where near-stoichiometric fuel-rich mixtures prevail up to a height of $h \approx 150$–180 mm. The spatial variations of the mixture fraction are rapidly smoothed out with increasing downstream position, for example from $f_{\text{min.}} = 0.008$, $f_{\text{max.}} = 0.653$ at $h = 10$ mm to $f_{\text{min.}} = 0.0480$, $f_{\text{max.}} = 0.0754$ at $h = 40$ mm. The numerical simulation with Fluent 5 leads to a mixture fraction distribution, displayed in the left-hand part of Fig. 6, which does not match the measured distribution. The reasons for this behavior must be attributed to deficiencies in the calculation of the turbulent velocity field: whereas the numerical calculation gives an open swirl flow core, the measurements reveal a more closed form with a small but intense central recirculation region [5, 18]. Neither variations of the inlet velocity profiles nor an exchange of the turbulence and combustion models employed (modified k-ε model, eddy dissipation concept) resulted in a significant improvement of the calculated results. Thus, at present the reasons for the shortcomings of the model calculations are unclear.

The corresponding temperature distributions are shown in Fig. 7. The highest mean temperatures are measured near the flame axis at $h \approx 40$–100 mm and are close to 2000 K with RMS fluctuations below 200 K. The high-temperature level in this part of the inner recirculation zone means that the gas has not experienced a considerable heat loss, i.e. it cannot have been in contact with a wall or radiated for a long time, and probably most of it has been transported directly from the flame zone to this region. Also, in laser light sheet measurements it was seen that significant OH concentrations are present in this region reaching down to the surface of the burner mouth. This finding reflects the stabilization mechanism of swirling flames which is based on the fact that hot gases with radicals are transported to the flame root within the inner recirculation zone. Due to the cold walls of the combustion chamber, the temperatures in the outer recirculation zone are substantially lower, e.g. $T \approx 1400$ K at $h = 150$ mm, and they drop with decreasing height. In the mixing region between the fuel and the air flow the temperature is quite low, e.g. $T \approx 300$ K at $h = 10$ mm, $r = 18$–30 mm. Although near-stoichiometric mixtures are present in this region they are not ignited because the hot gas from the inner recirculation zone is shielded from these mixtures by the cold natural gas flow (as discussed before). The comparison of numerically calculated and measured temperature fields shows the same behavior as found for the mixture fraction: large discrepancies are seen between the structures of the calculated and measured temperature fields.

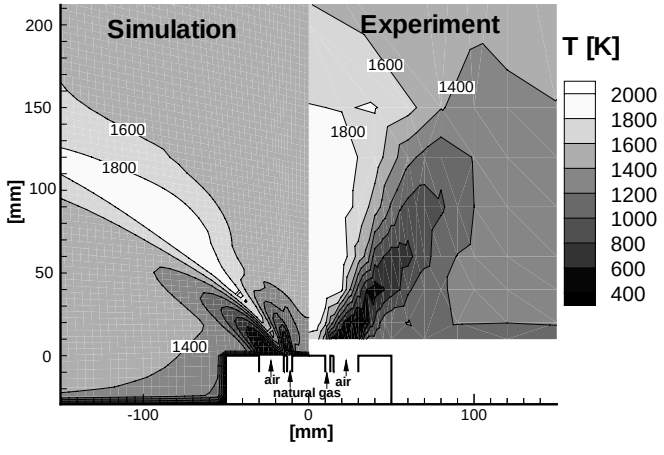

Fig. 7. Favre-averaged mean temperatures. *Right side*: experiment, *left side*: simulation. Only the central part around the burner mouth is displayed

4 Conclusions

Joint PDFs of temperature, mixture fraction, and major species concentrations have been measured by spontaneous Raman scattering in a confined swirling flame with 150 kW thermal load. The scatterplots of temperature, CH_4, and CO mole fractions give an insight into the thermochemical state of the flame and have been discussed in detail for the start region of the flame. Here, gas samples with reacted, unreacted, and partially reacted mixtures have been identified, and it was seen that pyrolysis plays a role in the layer between hot combustion products and natural gas. Also, the mixing behavior and the temperature reduction due to heat loss could be quantified. The measured mean mixture fraction and temperature fields reflect quantitatively the different regimes of the flame: the region of mixing between the fuel and air stream with low to medium temperatures and steep gradients of f, the inner recirculation zone with high temperatures and fuel-rich near-stoichiometric mixtures, and the outer recirculation zone with temperature-reduced exhaust gas.

The results from the simulation with the Fluent 5 code are unsatisfactory so far because the general behavior of the flow field cannot be predicted realistically. Thus, a really sensitive comparison between measurement and simulation could not be performed.

The presented investigations are part of the TECFLAM cooperation and the TECFLAM data archive also contains results from LDV measurements, two-dimensional Rayleigh scattering and laser-induced fluorescence, probe technique measurements, and thermal radiation detection, which are available on request.

Acknowledgements. The authors would like to thank their TECFLAM partners from the Engler-Bunte-Institut, Feuerungstechnik, in Karlsruhe for kindly providing the LDV data. The financial support from the Bundesministerium für Bildung und Wissenschaft within the TECFLAM project (BMBF 0327059A) is gratefully acknowledged.

References

1. TECFLAM web page, www.tu-darmstadt.de/fb/mb/ekt/tecflam
2. T. Landenfeld, A. Kremer, E.P. Hassel, J. Janicka, T. Schäfer, J. Kazenwadel, C. Schulz, J. Wolfrum: 27th Symposium (Int'l) on Combustion (The Combustion Institute, Pittsburgh 1998) p. 1023
3. S. Böckle, J. Kazenwadel, T. Kunzelmann, D.-I. Shin, C. Schulz: Appl. Phys. B **70**, 733 (2000)
4. S. Böckle, J. Kazenwadel, T. Kunzelmann, D.-I. Shin, C. Schulz, J. Wolfrum: 28th Symposium (Int'l) on Combustion (The Combustion Institute, Pittsburgh 2000) in press

5. P. Schmittel, B. Günther, B. Lenze, W. Leuckel, H. Bockhorn: 28th Symposium (Int'l) on Combustion (The Combustion Institute, Pittsburgh 2000) in press
6. F. Holzäpfel, B. Lenze, W. Leuckel: 26th Symposium (Int'l) on Combustion (The Combustion Institute, Pittsburgh 1996) p.187
7. W. Meier, S. Prucker, M.-H. Cao, W. Stricker: Combust. Sci. Technol. **118**, 293 (1996)
8. V. Bergmann, W. Meier, D. Wolff, W. Stricker: Appl. Phys. B **66**, 489 (1998)
9. S. Prucker, W. Meier, W. Stricker: Rev. Sci. Instrum. **65**, 2908 (1994)
10. R.W. Bilger: 22nd Symposium (Int'l) on Combustion (The Combustion Institute, Pittsburgh, 1988) p. 475
11. www.dlr.de/VT
12. B.E. Launder, G.J. Reece, W. Rodi: J. Fluid Mech. **68**, 537 (1975)
13. B.E. Launder: Inter. J. Heat Fluid Flow **10**, 282 (1989)
14. K.K.Y. Kuo: In *Principles of Combustion* (Wiley, New York 1986)
15. W.P. Jones, J.H. Whitelaw: Combust. Flame **48**, 1 (1982)
16. M.G. Carvalho, T. Farias, P. Fontes: Fundam. Radiat. Heat Transfer **160**, 17 (1991)
17. R. Koch, Universität Karlsruhe: private communication
18. P. Schmittel, Universität Karlsruhe: private communication
19. J.H. Miller, R.J. Kee, M.D. Smooke, J.F. Grcar: Paper WSS/CI 84-10, Western State Section of the Combust. Inst., Spring Meeting 1984
20. J.-Y. Chen, UC Berkeley: private communication
21. P. Glarborg, R.J. Kee, J.F. Grcar, J.A. Miller: Sandia Report 86-8209 (1992)